High Resolution Coronal Imager (Hi-C) observations of transverse waves in active region structures

R J Morton & J A McLaughlin
Northumbria University, UK

Introduction

There have now been numerous reports of ubiquitous magneto-hydrodynamic (MHD) waves in the solar atmosphere. In particular the periodic, transverse displacement of magnetic flux tubes in both the chromosphere [1-3] and in the corona [4,5]. The observations of coronal transverse waves are limiteded because of large spatial resolutions, >0''.5 per pixel, and also because the coronal plasma is optically thin. Both these effects contribute to problems with line-of-sight (LOS) integration, meaning that several coronal structures may contribute to emission within a single pixel. This limitation has led to some differing results on the observed properties of the transverse waves. For example, velocity amplitudes of these waves are reported as *~0.4 km/s* in off-limb, active region loops (*Coronal Multi-Channel Polarimeter/CoMP* [4]), while observations with the *Solar Dynamic Observatory (SDO)* suggest typical amplitudes of *5±5 km/s* [6]. To explain this, it was suggested that LOS integration of multiple unresolved structures would lead to an underestimate of velocity amplitudes [7].

The data taken with the *High resolution Coronal Imager* (*Hi-C* [8]) provides a unique opportunity of studying active region transverse waves at high resolution and thus revealing new information.

In addition, *Hi-C* allows for a detailed study of the moss regions [9,10], i.e., the upper Transition Region (TR) emission of high pressure loops in active regions. The moss appears as a reticulated pattern of bright emission in EUV images, with large-scale structuring on spatial scales of 2-3 Mm, with an apparent vertical extent of ~1-4 Mm [11]. The bright emission is punctuated with patches of low emission (dark inclusions) and, in general, the regions of low emission show a correlation with spicules observed in Hα wings [12]. However, previous instruments have not had adequate spatial resolution to resolve fine-scale structure in either the bright or dark regions.

Observations have revealed that moss emission varies little over extended time periods [13,14], with the implication that the heating must be quasi-steady in nature and dominated by continuous high-frequency heating events. This scenario has support from reports of high-frequency intensity variations in the moss, observed with *Hi-C* [9]. On the other hand, time variability of the moss could well be due to motions of the magnetic field rather than a direct signature of heating [14].

Observations and Data Reduction

The *Hi-C* observations took place on 11 July 2012 from 18:52:09 UT to 18:55:30 UT centred on an active region. The images were obtained in the 193 Å passband (spectral width 5 Å). The data were taken with a cadence of ~5.6 s and a spatial resolution of 0''.103 per pixel (~75 km).

The 193 Å line has strong contributions from Fe XII, which has a peak formation temperature close to 1.5 MK. The images not only show well-defined coronal loops but also spicular and fibrillar structures in and around the moss regions. The data reveals spicules/fibrils constantly in motion, displaying evidence of flows and waves. This is in contrast to a corona that shows relatively muted dynamic behaviour.

Due to the low signal-to-noise ratio (S/N) of *Hi-C*, a spatial filtering algorithm is applied to each frame to suppress the highest frequency components and increasing the S/N. To highlight the fine-structure an unsharp mask procedure is used.

Additional data from the *SDO Atmospheric Imaging Assembly (AIA)* [15] is used to study the long-term behaviour of the region. The data represent a larger region around the *Hi-C* field of view, comprise of the 171 Å and 193 Å bandpasses, and cover the period 18:40:47-19:04:47 UT.

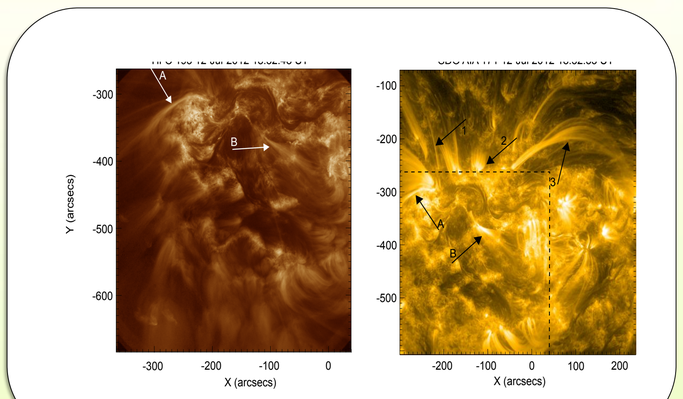

Figure 1. *Hi-C* (left) and *SDO/AIA* (right) fields of view. The dashed box shows the *Hi-C* field of view with respect to the *AIA* data.

Wave Fitting

Signatures of transverse wave motion are the physical displacement of the structure's central axis. To observe this, cross-cuts are placed perpendicular to the structure under consideration and a time-distance diagram is produced. At each time, a Gaussian function is fitted to the cross-sectional flux profile of the structures in the time-distance diagrams. The fitting of the Gaussian requires an estimate of the data noise (σ_N). We also take into account errors in alignment between the frames. The Gaussian centroids were fit with a function of the form

$$F(t)=A\sin(2\pi t/P-\varphi)+g(t),$$

where A, P, and φ are the displacement amplitude, period, and phase, respectively, of the wave. The parameter $g(t)$ is a linear function that represents any transverse drift of the structure with time, which could be attributed to long-period waves.

Waves in coronal loops

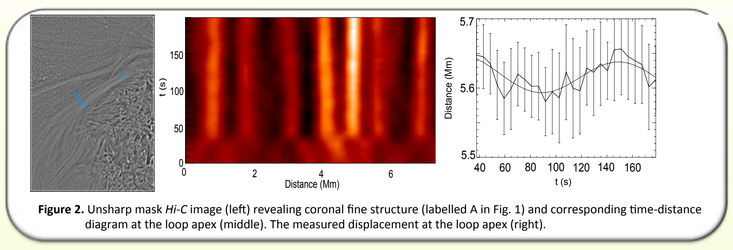

Figure 2. Unsharp mask *Hi-C* image (left) revealing coronal fine structure (labelled A in Fig. 1) and corresponding time-distance diagram at the loop apex (middle). The measured displacement at the loop apex (right).

Results from *Hi-C* - Numerous coronal structures can be observed in the *Hi-C* images. Two large, distinct coronal structures with large S/N are identified (Fig. 1 - labelled A and B). An example time-distance diagram for A is plotted in Fig. 2. Fitting a Gaussian to the loop cross-sections gives loop widths of *150-310 km*. Such fine structure is not clearly resolved in the corresponding *AIA* images.

Perhaps surprisingly, these structures show little visible evidence of periodic transverse motion. We are able to measure small amplitude transverse displacement towards the foot-points of the loops in structure A, where the measured displacement amplitude (*47±14 km*) is a factor of 10 smaller than the *AIA* pixel size. Cross-correlation of the signals in neighbouring slits suggests the feature is propagating with phase speeds *400±300 km/s*. Transverse motion in a neighbouring loop in the legs (Fig. 3) also has a small displacement amplitude of *A=22±12 km*, with *P=65±10 s*. The identification of periodic transverse displacement towards the loop apex is more uncertain because of lower S/N.

In the second coronal structure labelled B there is no measurable periodic motion. The results from the fitting hint at very small amplitude periodic motion below the errors.

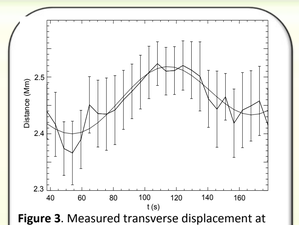

Figure 3. Measured transverse displacement at the foot-point of loop A. Error bars are σ uncertaintiesin loop position.

AIA Results - To gain a sense of typical wave activity in the active region, additional structures in the *AIA* 171 Å images were studied (labels 1-3 in Fig. 1). Fig. 4 displays the time-distance diagrams produced for these features. Measurements suggests the presence of long-period (*P > 300 s*) and small-amplitude (*A < 100 km, v < 3 km/s*) waves in structures 1 and 2. The feature labelled 3 is different and displays transverse motion in numerous loops that is visible even to the eye. An example is highlighted (black line) and the measured values are *P = 324 ± 2 s*, *A = 331 ± 4 km*, *v = 6.42 ± 0.1 km/s*.

Summary - The five-fold increase in resolution of *Hi-C* allows observation of transverse periodic motion (*A<50 km*) in coronal loops that would otherwise have been difficult with *AIA*. The *Hi-C* data reveals small-amplitude, low-energy waves, although some coronal structures do not show measurable periodic transverse motion even at high resolution.

Assuming the active corona is filled with transverse waves, our results allow an upper bound to be placed on the amplitude of the transverse waves in some active region loops. We suggest that transverse waves with an amplitude of *< 0''.03* (*20 km*) are at the edge of *Hi-C* observational limitations. Hence, any waves present with periods in the range *20-200 s* will have velocity amplitudes of *< 6 km/s*.

Comparing *Hi-C* to extended time-series taken from *AIA* suggests that the period of time observed by *Hi-C* is representative of the dynamics in the structures studied, i.e., waves typically have a small velocity amplitude . This implies that transverse waves supported by some active region coronal structure would not provide a significant heating contribution.

The larger amplitude waves in feature 3 appear to be an individual case and their presence could be a sign that a large energy release has occurred, e.g., reconnection.

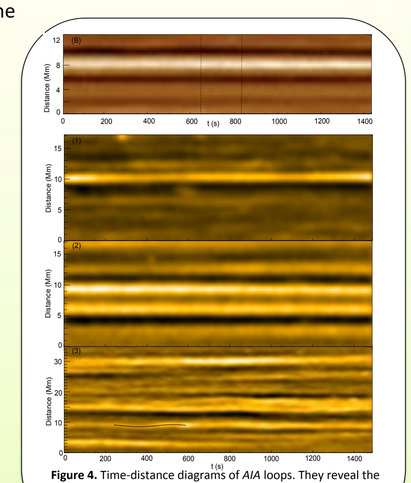

Figure 4. Time-distance diagrams of *AIA* loops. They reveal the lack of wave motion in coronal loops (first 3 panels). The bottom panel shows a loop arcade in which measureable waves exist.

Fine-scale structure in moss regions

Figure 5 shows a close up of a moss region in *AIA* 304 Å, 171 Å and 193 Å bandpasses. The *AIA* images show that small-scale structuring in the moss regions is present but it is clearly unresolved. In Figure 6, we display an image taken with *Hi-C* that focuses on a particular patch of the moss. The fine structuring is now evident but its presence is clearer after passing the data through an unsharp-mask routine. The *Hi-C* data reveals that the moss emission is located at the visible, upper ends of a collection of fine threads, whose emission highlights the underlying magnetic field. The structures are visible in the dark inclusions, hence have reduced emission relative to the bright moss. Further, the structures appear to extend into the lower solar atmosphere. The particular region of interest is essentially a gap in the moss, where the collection of fine structure opens-up, with groups of structures inclined in different orientations. This gap due to the structure's inclination allows the lower extensions of the bright moss to be observed.

In order to reveal the typical scale of the fine structures, we select features from each of the identified moss regions and measure their widths in the *Hi-C* data. The fine structure in unsharp masked images are fitted with a combination of a Gaussian function and a linear function. In Figure 6 we display both the σ values of the Gaussian and the Full-Width-Half-Maximum (*2√(2ln(2)) σ≈2.35σ*) values. The measured widths are comparable to the results obtained for coronal loops [16] and for chromospheric structures [2].

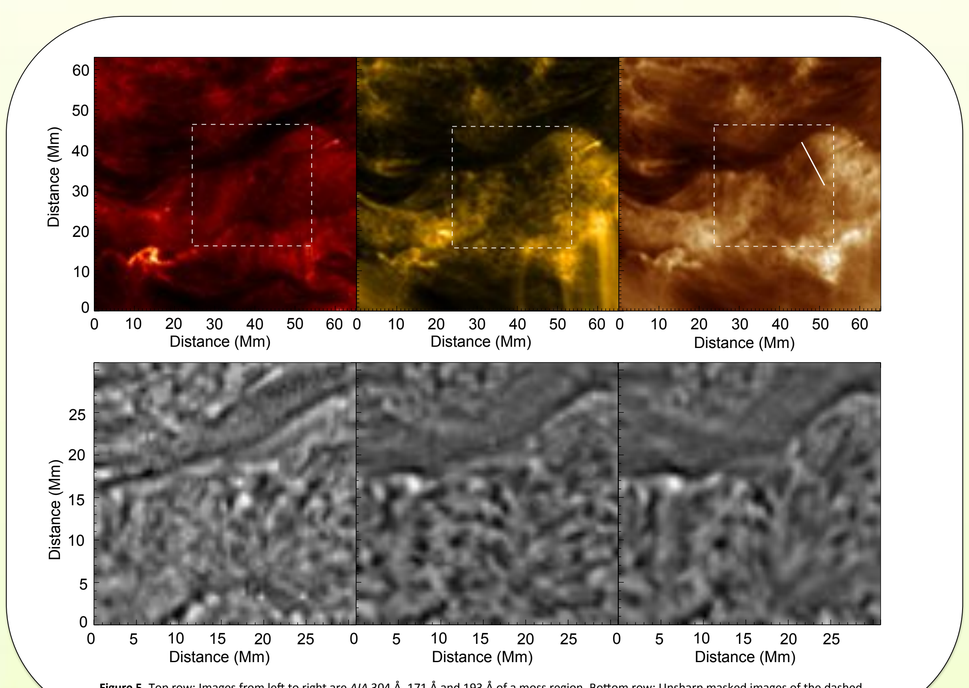

Figure 5. Top row: Images from left to right are *AIA* 304 Å, 171 Å and 193 Å of a moss region. Bottom row: Unsharp masked images of the dashed boxed regions.

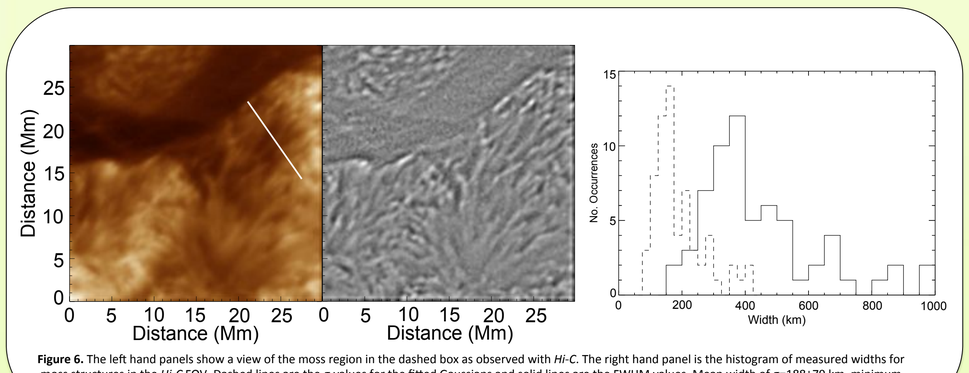

Figure 6. The left hand panels show a view of the moss region in the dashed box as observed with *Hi-C*. The right hand panel is the histogram of measured widths for moss structures in the *Hi-C* FOV. Dashed lines are the σ values for the fitted Gaussians and solid lines are the FWHM values. Mean width of σ=188±79 km, minimum σ=76 km and maximum σ=414 km.

Waves in moss regions

Being able to resolve the fine structure now allows for the examination of the dynamic behaviour in the moss regions. In particular, we are interested in whether there are signatures of MHD waves in the Transition Region, more specifically the presence of kink (Alfvénic) waves. We find 68 measurable examples of transverse wave behaviour in the *Hi-C* time-series. The waves are observed in the structures that generally have greater emission than their surroundings, suggesting the waves exist in the Transition Region rather than the EUV absorbing/blocking chromospheric material that occurs occasionally between the fine-structure. The ability to observe waves in the dark inclusions is limited in part due to the low S/N levels in these regions and partially due to the small displacement amplitude (~50 km) of the waves. The presence of waves in the moss has been conjectured [13, 14] and it is thought that the waves will cause some of the observed variability in the cores of the active region moss rather than heating events. Examples of the observed waves are displayed in Figure 7.

From the time-distance diagrams it is possible measure the transverse displacement amplitude (*A*) and the period (*P*) of the waves. The velocity amplitude, *v*, is given by $v=2\pi A/P$ and the average velocity power, *W*, for the waves, $W=v_{rms}^2/f=v^2P/2$ where v_{rms} is the root-mean-square velocity and $f=1/P$ is the frequency of the wave. The measured properties of all waves are given in Figure 8. Next, the data is fit with power laws of the form $10^a P^b$ for displacement amplitude and velocity amplitude and $10^c f^d$ for the velocity power, where *a, b, c* and *d* are unknown values to be found for the fitting to each individual quantity. The fit is calculated by binning in the frequency domain and the weighted mean and standard deviation are calculated for each bin. Furthermore, we estimate the observational constraints based on the cadence of the instrument and the wave measurement technique.

The measured properties of the waves are similar to those measured in spicules and fibrils [1,16,17]. Moreover, the measured velocity amplitudes of the waves here are greater than those typically reported in observations of coronal kink waves [4, 5], which implies that kink waves are more energetic in the lower solar atmosphere compared to the corona. The differences in energy and Poynting flux between the chromospheric and Transition Region waves can calculated using the measured values of the wave properties (i.e., amplitude, phase speed, etc.). The estimates suggest that the Transition Region Poynting flux is 50 % smaller than that in the chromosphere. Reported values of chromospheric energy flux are ~4000 W m^2, hence there is still a significant wave energy flux in the active region Transition Region. However, the overall wave energy is found to have decreased by 80%.

Figure 7. Examples of time-distance diagrams revealing MHD wave phenomenon in active region moss features. Over plotted black lines indicate the fits to the waves.

Figure 8. The frequency dependency of measured wave quantities. From left to right, the plots show transverse displacement and velocity amplitude as a function of period and the velocity power as a function of frequency. The horizontal and vertical error bars correspond to the σ errors on each measured quantity. The blue lines correspond to weighted fits to the frequency binned means. The dotted lines correspond to the estimated observational constraints. The correlation coefficients for each scatter plot are also given in the top right hand corners.

Summary

While the calculated energy fluxes suggest the contribution of the kink waves to heating in hot loops will not be insignificant, the current observations do not allow for a more concrete statement to be made. The estimates for wave energy flux in the Transition Region do not rule out waves as a significant contributor to the active region heating budget. The continuous driving of waves via granular motions could provide the required quasi-steady heating mechanism in active regions. Alternatively, the observed waves could be the by-product of small-scale magnetic reconnection events, i.e., the classic nano-flares. It is well known from simulations of large-scale reconnection events that a fraction of the energy released is converted to wave energy [18]. An extended statistical study of wave propagation from the chromosphere to the corona will be able to provide a clear and unequivocal picture of wave propagation through the atmosphere.

References

[1] De Pontieu et al., Science, **318**, 1574 (2007)
[2] Morton et al., Nature Comms., **3**, 1315 (2012)
[3] Kuridze et al., ApJ, **750**, 51 (2012)
[4] Tomczyk et al., Science, **317**, 1192 (2007)
[5] Erdelyi & Taroyan, A&A, **489**, L49 (2008)
[6] McIntosh et al., Nature, **475**, 477 (2011)
[7] De Moortel & Pascoe, ApJ , **746**, 31 (2012)
[8] Cirtain et al., Nature, **493**, 501, (2013)
[9] Testa et al., ApJ, **770**, L1 (2013)
[10] Winebarger et al., ApJ, **771**, 21 (2013)
[11] Berger et al., ApJ, **519**, L17 (1999)
[12] De Pontieu et al., ApJ, **590**, 502 (2003)
[13] Antiochos et al., ApJ, **590**, 547 (2003)
[14] Brooks & Warren, ApJ, **703**, L53 (2009)
[15] Lemen et al., Sol. Phys. **115** (2011)
[16] Morton et al., ApJ, **768**, 17 (2013)
[17] Morton et al., ApJ, Submitted (2013)
[18] Yokoyama & Shibata, PASJ, **48**, 353 (1996)